Contents list available at IJRED website

International Journal of Renewable Energy Development

Journal homepage: https://ijred.undip.ac.id

Research Article

A Brief Study on the Implementation of Helical Cross-Flow Hydrokinetic Turbines for Small Scale Power Generation in the Indian SHP Sector

Jayaram Vijayan[a*] and Bavanish Balac Retnam[b]

[a] *Department of Mechanical Engineering, Noorul Islam Centre for Higher Education, Tamil Nadu, India*

[b] *Department of Fire Technology and Safety Engineering, Noorul Islam Centre for Higher Education, Tamil Nadu, India*

Abstract. This article addresses the simulation and experiments performed on a Gorlov Helical Turbine (GHT) by altering the index of revolution of its helical blades. Gorlov Helical Turbine is a hydrokinetic turbine that generates energy from the perennial/tidal source. The paper serves a two-fold purpose: parametric optimisation of Gorlov Helical Turbine with respect to the index of revolution and viability of installing the turbines in river creeks. Nine models of turbines with a diameter of 0.600 m and a height of 0.600 m were generated with different indices of revolution and then subjected to simulation studies. A significant rise in the output torque of the turbine was not observed with the various indices of revolution, even as the probability of finding a section at every azimuthal position is likely to rise. Gavasheli's solidity ratio formula was used to formulate an expression for the output power. The output power as per analytical formulation is 1.11 W, which is of the order of output power obtained through simulation (0.951 W). The studies suggest that 0.25 remains the optimum value for the index of revolution of the helical blades. A model with 0.25 as the index of revolution was fabricated and tested at a river creek. The results were found to agree with the simulations accounting for the losses. The study results could encourage setting up hydrokinetic turbines in river creeks, thereby increasing the grid capacity of SHPs in India.

Keywords: Gorlov Helical Turbines (GHT), Index of revolution, Simulation, Experimentation, Turbulence Model, Optimization, Renewable energy

Received: 7th March 2022; Revised: 13th April 2022; Accepted: 16th April 2022; Available online: 25th April 2022

1. Introduction

Electrification has led to the rapid transformation of life in all aspects of modern civilisation. The need for more power has led to the development of various techniques for transforming energy from natural power sources into electricity (Mwaniki *et al.* 2019). The excessive use of fossil and nuclear fuels has forced many developing countries to implement modern renewable-energy based technologies at an agile rate. Ocean and perennial sources (currents) are among the most accessible renewable energy sources. The tidal/perennial energy, compared with other clean energy sources such as wind, sun and geothermal, is continuous and foreseeable for the future. Hydropower is an important source of renewable energy. The potential not only rests in the vast reservoirs but also in the oceans and river creeks in the form of currents. Conventional turbines are well suited for low discharge- high head or high discharge-low head applications. However, they are futile in ultra-low head applications. Another potential area is the tailrace water. The hydropower potential from such systems is often left untapped, as it is thought to be uneconomical. Hydrokinetic turbines are the best choice for such sources. Hydrokinetic turbines require no reservoir or spillway, making the design and construction simple. Hydrokinetic turbines can be categorised as axial and cross-flow based on the current flow and orientation of the turbine axis. Axial-flow hydrokinetic turbines feature a rotational axis that is horizontal/inclined or parallel to the direction of water flow. Axial-flow turbines are more suited to applications such as ocean currents. In cross-flow hydrokinetic turbines, the rotational axis is always orthogonal to the incoming flow of water. The cross-flow turbine's cylindrical design enables more efficient use of the depth of the channel. The cross-flow turbine is often known for its self-starting capability. Cross-flow turbines are further categorised into vertical axis cross-flow hydrokinetic turbines and horizontal axis cross-flow hydrokinetic turbines. Horizontal axis cross-flow turbines are well suited for applications in shallow water. In comparison, vertical axis cross-flow hydrokinetic turbines are suitable for a greater water depth. Savonius (Mrigua *et al.* 2020) and Darrieus turbines (Yagmur *et al.* 2021) are two simple vertical axis cross-flow turbines. The other

* Corresponding author
Email: jayaramvijayan@gmail.com (Jayaram.V)

https://doi.org/10.14710/ijred.2022.45249
ISSN: 2252-4940/© 2022.The Author(s). Published by CBIORE

classes of turbines, such as the H-Darrieus, Squirrel cage, Lucid turbine, and Gorlov, are modified versions of Darrieus turbines.

As per the Energy statistical report - 2021 released by the National Statistical Office (Government of India), India's total renewable energy reserve is 1,097,465 MW. Small hydropower constitutes only 1.93% (21,134 MW) of the reserve. As per Indian standards, Small Hydel Power plants are those whose capacity is between 2 MW and 25 MW. Over the years, the contribution of small hydropower (Ravikumar *et al.* 2020) towards cumulative hydropower has not changed much, owing to the reluctance to identify and adopt better technology. Cross-flow hydrokinetic turbines could be employed in canal systems, tailrace of irrigation dams and smaller river streams, thereby enhancing the share towards the small hydropower sector. The study is intended to evaluate the performance characteristics of the Gorlov helical turbine and its viability of implementation. The Gorlov helical turbine is a water turbine based on the design of the Darrieus turbine. The vertical blades of the Darrieus turbine were replaced with helical blades of aerofoil cross-section, which offers better performance. The Gorlov helical turbine (Gorlov, 1998) is an efficient, budget-full, and ecological reaction turbine for deriving hydropower from free (kinetic) and low head (potential) water streams. This is a relatively emerging technology, but the turbine has already been installed in several tide potential country seashore sites. The project implemented in Uldolmok Strait (South Korea) is one of the oldest (Figure 1).

Gorlov, (1998) evaluated the performance of a three-bladed Gorlov helical turbine measuring 24 in. (0.6096 m) in diameter and 34 in. in height (0.8636 m). For stability, Gorlov used a NACA0020 aerofoil with a 7 in. (0.1778 m) chord. The turbine had an efficiency of 35% for a flow rate of 1.54 m/s. Shiono et al (2002) evaluated four distinct types of helical blades of a Gorlov helical turbine. The solidity of the turbine blades was varied from 0.20 to 0.50 with a 0.1 increment, keeping a constant diameter and height (AR=1). While solidity significantly affected starting characteristics, the blade inclination angle showed no such effect. The highest efficiency was observed for the turbine with a solidity of 0.4.

Talukdar *et al.* (2018) evaluated the performance of the Gorlov helical turbine by varying the solidity ratio. In-situ testing of the turbines in an open channel revealed that the turbine with a solidity ratio of 0.38 developed a maximum power coefficient of 0.20 at a TSR of 1.02 for a velocity of 0.87 m/s. The effect of the solidity ratio on the turbines' performance was also examined for different immersion levels. The power coefficient was found to decrease with a decrease in immersion depth. This effect was pronounced in turbines with a lower solidity ratio (σ=0.31).

(Pongduang, Kayankannavee & Tiaple. 2015) studied the effect of the helical angle on the performance of the Gorlov helical turbine. Two tidal turbines of diameters 0.5 m and 0.6 m (height = 1.25 m) were tested in a towing tank. The profile of the blade was NACA0020 (0.07 m chord length). Testing of three-bladed models with a helical angle of 120^o, 135^o, and 150^o was conducted for different flow conditions. Studies concluded that the model with a helical angle of 135^o performed efficiently for a TSR range of 2.2 to 2.5.

Kirke, (2011) studied the effect of variable pitch on straight and helical bladed hydrokinetic turbines. The variation in pitch is known to improve starting torque and efficiency. However, only two pitch values (5^o and 10^o) were studied. Studies suggest that the turbine with 100 pitch had a C_p around 0.4.(Mosbahi *et al.* 2020) carried out numerical and experimental studies on Darrieus turbine with delta blades. The turbine's performance was numerically evaluated for leading-edge sweep angles varying from 10^o to 40^o. The best results (leading-edge sweep angle=30^o) were experimentally verified. The numerical methodology adopted in the current paper is from (Mosbahi et al. 2020) and (Shashikumar *et al.* (2021a); Shashikumar *et al.* (2021b); Shashikumar & Madav. (2021)).

This literature survey indicates that various experimental and computational investigations on the Gorlov helical turbine have been conducted to determine its performance using C_p, C_t, and solidity ratios. However, the effects of helical angle and pitch of the blade are not well assessed. (Pongduang, Kayankannavee & Tiaple. 2015) conducted the only study on the helical angle, focusing exclusively on 120^o, 135^o, and 150^o. Similarly, the survey by (Kirke B, 2011) on the pitch of the turbine blade is also confined to two specific values (5^o and 10^o).

The current research proposes evaluating the turbine's performance using the 'index of revolution', the function of pitch and helical angle. In the present study, a numerical analysis is conducted on Gorlov helical turbine by varying the index of revolution (from 0.1 to 0.5 with an increment of 0.05) for similar flow conditions and further experimentally validated. The field testing will put insight into the viability of implementing Gorlov helical turbines in river creeks.

Fig 1. Gorlov Helical Turbines being installed in South Korea (Chakka, 2015)

Table 1
Correlation between pitch and index of revolution

Height of the turbine (m)	Pitch of the helix (m)	Index of revolution
0.600	6.000	0.10
0.600	4.000	0.15
0.600	3.000	0.20
0.600	2.400	0.25
0.600	2.000	0.30
0.600	1.714	0.35
0.600	1.500	0.40
0.600	1.333	0.45
0.600	1.200	0.50

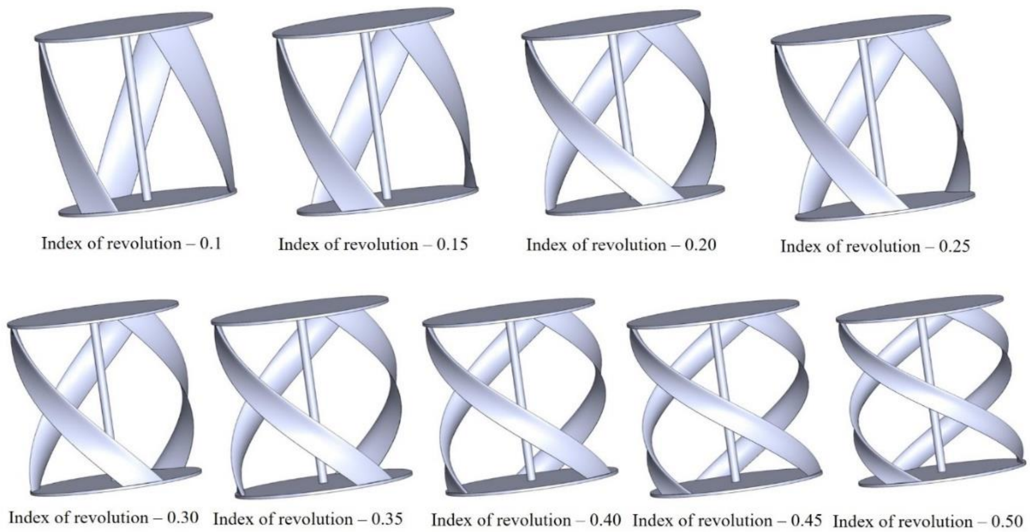

Fig. 2 GHT's with different indices of revolution (Jayaram & Bavanish. 2018)

2. Analytical model

The study investigates the parametric optimisation of GHT with respect to the index of revolution (Bachant & Wosnik. 2011) and further a methodology to implement them in a perennial/tidal source. Even though there are various parameters to be optimised, such as helix angle and solidity ratio (Supreeth *et al.* 2019), the effort has been concentrated on the helical blade profile's index of revolution (pitch). Index of revolution may be defined as the fraction of the pitch of one complete helix turn measured parallel to the axis and fitted between the turbine discs (refer Figure 2, 4).

A 3-D model, as illustrated by (J.Zanette, D. Imbault & A. Tourabi. 2010), was created using SolidWorks and subjected to the cross-flow velocity of 1.5 m/s. Since a helical cross-flow turbine is known for its automated self-starting capability, no rudders were provided. The parameters governing helical turbine design include the radius of the disc, blade cross-sectional geometry (profile), helical-pitch angle, aspect ratio, number of blades, solidity ratio and design of strut are suggested by (Anderson *et al.* 2011). The study was concentrated on the revolution index (pitch) in this research work. The index of revolution was incremented by a value of 0.05 until half of the total revolution of the helix was reached. In all cases, the pitch of the helix had to be decreased to readjust the model's geometry (height being fixed to 0.600 m). Details of pitch and index of revolution are given in Table 1.

For optimum performance, as mentioned in literature and experiment (Gorlov, 1995), the number of blades was decided as 3. Unlike in the other experiments, the NACA 4412 with a 0.120 m chord was chosen as the blade profile. Even though S1210 appears to have the edge over NACA 4412, it is difficult to manufacture. Figure 3 depicts the comparison of various standard profiles employed for the above purpose. The height of the helical sweep is usually taken as three times the turbine height. For instance, for a turbine height of 0.600 m, the helical sweep height would be 1.800 m.

In the initial phase of the study, a set of simulations was conducted with varying heights to have an idea of optimum height. The turbine's height was varied from 0.500 m to 0.900 m in steps of 0.050 m (9 Models). The model with 0.600 m height performed better in terms of torque. The next phase involved modelling nine Gorlov Helical Turbines with a diameter of 0.600 m and a height of 0.600 m. Every model had a different index of revolution (starting from 0.10 and ending with 0.50, refer Figure 2). Figure 4 illustrates the profile of the path curve of the blade.

Additional simulations for all turbines of indices of revolution (0.10 to 0.50) were conducted with input flow velocities varying from 1.1 m/s to 1.7 m/s to establish the relationship between C_p and TSR. The physical/ Analytical calculations suggested by (Jayaram & Bavanish. 2018; Jayaram & Bavanish. 2020) of the Gorlov turbine are as follows:

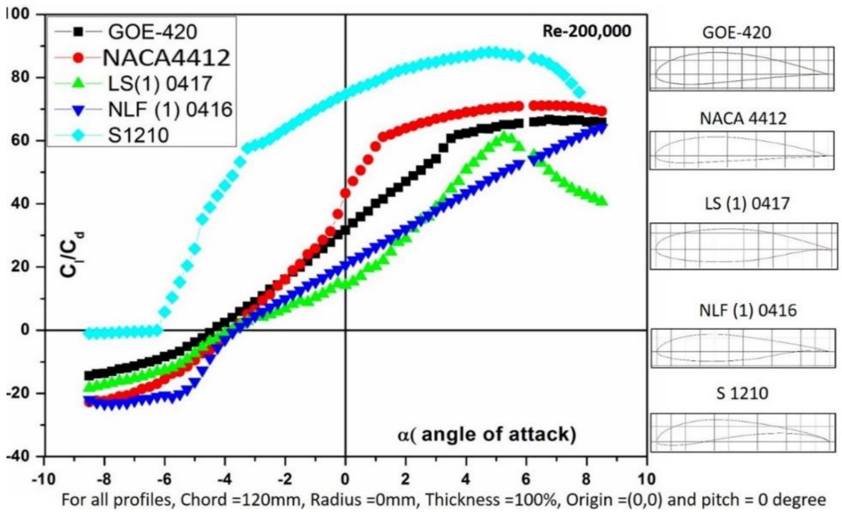

Fig. 3 Comparison of various aerofoil profiles of GHT

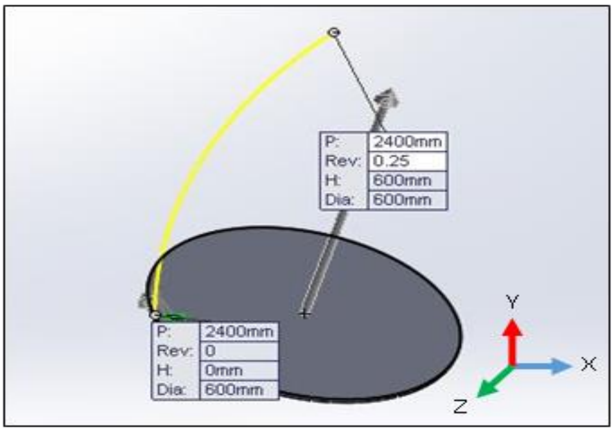

Fig 4. Profile of blade with 0.25 as the index of revolution

The most frequently used geometrical characteristic of the turbine is its relative solidity, defined as the ratio

$$\sigma = \frac{nb}{D} \tag{1}$$

Solidity ratio indicates the proportion of the turbine's diameter that is solid compared to the entire circumference. In short, it refers to the effective frontal area resisting the fluid. The solidity ratio is often employed to find the tangential force acting on the turbine. M. Gavasheli and (Gorlov, 1995) derived an equation to evaluate the solidity ratio in blade area projections on the turbine shaft plane. Indicating the helical turbine's solidity by P (in terms of blade projection on the lateral plane),

$$P = \frac{2nHr}{\pi}(d + \sum_{j=1}^{n} sin(\frac{j\pi}{n} - d) - sin\frac{j\pi}{n}) \tag{2}$$

The relative solidity of the turbine σ = P/2Hr is calculated as follows:

$$\sigma = \frac{n}{\pi}(d + \sum_{j=1}^{n} sin(\frac{j\pi}{n} - d) - sin\frac{j\pi}{n}) \tag{3}$$

For example, for a four-blade turbine configuration, the relative solidity would be:

$$\sigma = \frac{4}{\pi}(d + sin(\frac{\pi}{4} - d) - sin\frac{\pi}{4} + sin(\frac{\pi}{2} - d) - sin\frac{\pi}{2} + sin(\frac{3\pi}{4} - d) - sin\frac{3\pi}{4} + sin(\pi - d) - sin\,\pi) \tag{4}$$

Further simplification of the equation involves incorporating the value of 'd' in terms of the chord (in radians). We opted for triple-blade configuration due to its self-starting characteristics, and hence the expression for relative solidity is:

$$\sigma = \frac{3}{\pi}(d - \sqrt{3} + sin\,d + \sqrt{3}\,cos\,d) \tag{5}$$

Further, in order to find the tangential force on the turbine the following formula is employed:

$$F = \frac{1}{2}C_d \rho \sigma A V^2 \tag{6}$$

The force is partially due to pressure exerted by the moving fluid on the projected area estimated with a relative solidity ratio. The torque is calculated according to equation (7)

$$T = 0.5FD \tag{7}$$

Formulas are used for the tangential drag force, torque, and power developed by the turbine, as indicated above. A primary study on the tangential force of the turbine blades was made for a whole set of parameters, including turbine, blade chord length, etc.

Knowing the value of the Tip Speed Ratio (TSR), the turbine's angular/rotational velocity can be estimated as:

$$\omega = 2V\lambda / D \quad (8)$$

The power of the turbine can be estimated using the idealistic formula

$$P_{ideal} = T \times \omega \quad (9)$$

However, in actual practice, the shaft power of the turbine and the final output will be further reduced due to mechanical transmission losses, gearbox efficiency (η_m) and generator efficiency(η_e). The equation can be modified according to equation (10)

$$P_{actual} = C_p \eta_m \eta_e P_{ideal} \quad (10)$$

The coefficient of power in the above equation can be estimated using:

$$C_p = \frac{T\omega}{\frac{1}{2}\rho\sigma A V^3} \quad (11)$$

The Tip Speed ratio can be estimated using:

$$TSR = \frac{\omega R}{V_f} \quad (12)$$

The model meant for simulation and experimentation had 0.120 m chord length and 0.600 m height and diameter. The TSR had a value of 1.00 for sampling measurements (usually varied between 0.5 & 2.5). For a turbine with three blades, the relative solidity is given by: $\sigma = \frac{3}{\pi}(\frac{1}{5} - \sqrt{3} + sin(\frac{1}{5}) + \sqrt{3}\,cos(\frac{1}{5}))$ and σ = 0.1943. This implies that a flow resistance is made available by 19.43 % of the overall estimated turbine's frontal area. The frontal area of the turbine without considering relative solidity, A= H x D = 0.360 m^2.

An unsymmetrical aerofoil -NACA 4412 was considered for the profile of the helical blades, as mentioned in section 2 with an average drag coefficient of 0.03627. Recalling Equation (6), the tangential force on the turbine: F= 2.85 N and $\omega = 2V\lambda / D$ = 5.00 rad/s, Turbine power, $P_{ideal} = F \times \omega \times (D/2)$ = 4.275 W

In practice, the turbine's shaft power and final output will be lowered further due to mechanical transmission losses, gearbox efficiency, and generator efficiency (refer equation 10). The standard estimate is 25%. The actual power is: P_{actual} = 1.11 W

3. Simulation

3.1. Creation of geometric model for simulation

The GHT is complex to model due to its helical blades. SolidWorks modelling module was chosen to draft the model due to its ability to handle complex surface profiles. An open-source web module (www.airfoiltools.com) generates the spatial points for NACA 4412 for a chord length of 0.12 m. The aerofoil profile is created using the points, as shown in Figure 5. The aerofoil profile (NACA 4412) as presented by (Camocardi *et al.* 2011) is etched onto the bottom disc of the GHT. We arbitrarily set the angle of attack of the blades as zero. In the next step, the sweep profile feature is used to achieve the required trajectory of the helical blades, as illustrated in Figure 6A.

The height and index of the revolution of the turbine can be varied at this phase of modelling (refer to Figure 6 B). A parallel plane is mirrored at the required height, as shown in Figure 6C. The second disc with the diameter as same as the former is drafted in this plane. This is illustrated in Figure 6D. The circular pattern feature is then applied with respect to the local Z axis. The number of blades is set as three. This is illustrated in Figures 6 E and 6 F. The front view of GHT is shown in Figure 7, with critical geometric features such as height (H), diameter (D), and helical blades highlighted.

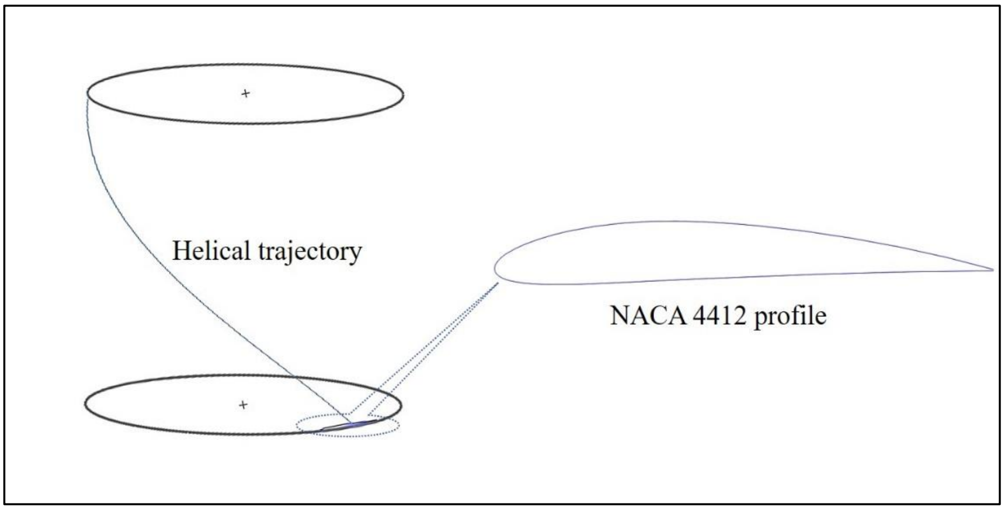

Fig. 5 Profile generation using SolidWorks

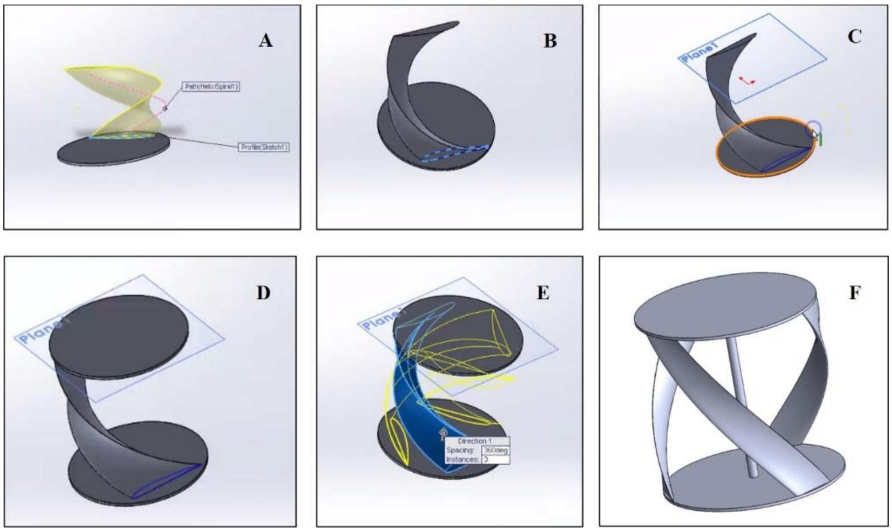

Fig. 6 Various stages in modelling GHT

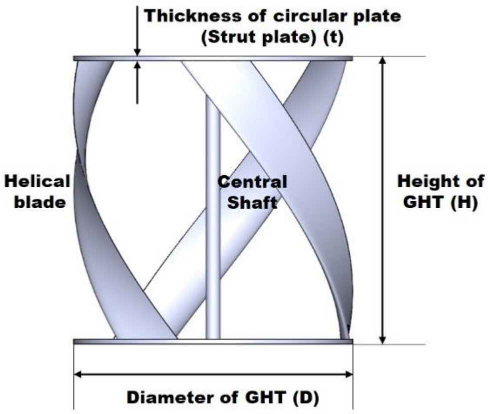

Fig. 7 3-D model of the GHT with all geometric parameters (front view)

3.2 Computational domain

Figure 8 shows the three-dimensional computational domain equivalent to an open channel of a river creek modelled with SolidWorks FSM (Flow Simulation Module). The computation domain has four walls: bottom, left, right, and a top surface open to the atmosphere. The computational domain's total length (from inlet to outlet faces) is fixed at five times the GHT's diameter (5D) as suggested by (Rezaeiha. A, Ivo Kalkman and Bert Blocken. 2017). The GHT is positioned at 2.5 times the GHT's diameter (2.5D) from the inlet and outlet of the computation domain's (centre of the domain). GHT, rotating region (turbine enclosure), and outer fluid region (river creek) are the three principal zones of the computational domain. The domain's width is set to three times the diameter of GHT (3D). The GHT is equally spaced in the lateral direction. Based on the literature (Rezaeiha. A, Ivo Kalkman and Bert Blocken. 2017; Dabbagh & Yuce. 2018; Dabbagh & Yuce. 2019), the size of the rotating zone throughout this simulation is 1.5 times the GHTs diameter. Table 2 shows the major computational domain dimensions such as the width of the domain (W_d), length of the domain (L_d), depth of the domain (D_d), turbine diameter (D), and rotating region diameter (D_r).

3.3 Details of mesh used for computation.

The geometric model (GHT) created using SolidWorks was imported into the Flow Simulation Module (FSM) of SolidWorks (Driss *et al.* 2014; Oliveira, Bernardo & Sundnes. 2016; Letchumanan *et al.* 2021; Singh & Nataraj. 2014; Prabhu *et al.* 2002; Akhatova *et al.* 2015). The solver assigns computational domain and necessary features with hexahedral mesh by default. A fine mesh is applied to the rotational region and the outer region with a coarse mesh. (Oliveira, Bernardo & Sundnes. 2016) suggested that hexahedral (or quad) meshes are often more efficient for wall-bounded flows, as orthogonal grids are preserved in the wall-normal direction. The hex elements are more precise, as the angle between faces may be kept near 90 degrees. When the Reynolds number is high, the spacing in the wall-normal direction must be highly refined. Hex grids enable excellent wall-normal spacing while avoiding excessive face skewness. The hex mesh offers an advantage over other mesh types in mesh refinement. The refinement level is set to the maximum level 5 (rotating region) to minimise mesh distortion along the curved surface. The hex elements near the surface are refined (thereby eliminating inflation) to capture the boundary effects. The maximum, minimum and average sizes of meshes are $1x10^{-3}$ m, $1.653x10^{-5}$ m, $0.8368x10^{-3}$ m, respectively. The value of y plus (y+) is 0.9879 (less than one). The mesh quality parameters such as aspect ratio and Jacobian ratio are 1 and 4, respectively. These values are within the acceptable range (Driss *et al.* 2014; Price & Armstrong. 1995). The meshed computational domain, the rotational region and inflation layer are illustrated in figure 9.

3.4 Mesh independence study

The effect of the number of mesh elements on the turbine's performance index (coefficient of power, C_p) was investigated using simulations for a flow velocity of 1.5 m/s. (Gorlov, 1998; Shiono, Suzuki & Kiho. 2002; Mosbahi *et al.* 2020; Berhanu *et al.* 2021; Shashikumar *et al.* (2021b))

The turbine with an index of revolution of 0.25 was opted for the study. Six mesh models were used to achieve mesh independence: K_1, K_2, K_3, K_4, K_5, and K_6 with mesh elements 1186922, 1285109, 1499780, 1556050, 1639761, and 1743910, respectively. In Figure 10, the power coefficient of GHT with 0.25 as the index of revolution is plotted against the number of mesh elements. A closed-form solution of $C_p = 0.2463$ corresponding to the criterion mentioned above was used for the error estimation (Mosbahi *et al.* 2020; Shashikumar *et al.* (2021a); Bachant & Wosnik. 2011). There was no significant difference in the value of C_P when the number of mesh elements was increased beyond K_4 (refer to figure 10). As shown in Table 3, the meshing models K_4 and K_5 have the lowest error values. Thus, to maximise the efficiency of the numerical investigations, the K_4 mesh model was used.

3.5 Governing equation and turbulence modelling

SolidWorks Flow Simulation Module (FSM) is a comprehensive parametric flow simulation tool that calculates a product's performance using the finite volume method (FVM). The FSM solves Navier-Stokes (NS) equations in fluid regions, which are representations of the mass, momentum, and energy conservation laws (Equations 13-15).

$$\Delta \cdot (\bar{\rho}\bar{V}) = 0 \tag{13}$$

$$\bar{\rho}(\bar{V}\cdot\nabla)\bar{V} = -\nabla\bar{p} + \mu\nabla\cdot(\nabla\bar{V} + \bar{\rho}(\bar{V}\cdot\nabla)\bar{V}^T) - \frac{2}{3}\mu\nabla(\nabla\cdot\bar{V}) + f(t) \tag{14}$$

$$\bar{\rho}(\bar{V}\cdot\nabla)(c_V\bar{T}) = K\nabla^2\bar{T} - p(\nabla\cdot\bar{V}) + \mu\phi + f(t) \tag{15}$$

SolidWorks FSM is dedicated to turbine simulation (where the flow is usually turbulent). One of the most prevalent turbulence models is the two-equation model. FSM uses the K-ε model (two-equation model) for computation as suggested by (Driss *et al.* 2014) and (Putra, Noviani & Muhardi. 2022). FSM is capable of taking into account both laminar and turbulent flows. Laminar flows exist at low Reynolds numbers, defined as the product of flow velocity and length scales divided by the kinematic viscosity. When the Reynolds number surpasses a predetermined critical value, the flow becomes turbulent. The Favre-averaged NS equations are employed to forecast turbulent flows, which consider the time-averaged implications of turbulence on the flow parameters while ignoring large-scale, time-dependent events. This approach introduces new terms called Reynolds stresses into the equations, requiring further information. FSM uses the K-ε model (turbulent kinetic energy and its dissipation rate) to close this system of equations.

$$\frac{\partial(\rho k)}{\partial t} + \frac{\partial(\rho k u_i)}{\partial x_i} = \frac{\partial}{\partial x_j}\left[\frac{\mu_t}{\sigma_{k1}}\frac{\partial k}{\partial x_j}\right] + 2\mu_t\xi_{ij}^2 - \rho\xi \tag{16}$$

$$\frac{\partial(\rho\xi)}{\partial t} + \frac{\partial(\rho\xi u_i)}{\partial x_i} = \frac{\partial}{\partial x_j}\left[\frac{\mu_t}{\sigma_{\xi1}}\frac{\partial\xi}{\partial x_j}\right] + 2.88\frac{\xi}{k}\mu_t\xi_{ij}^2 - 1.92\rho\frac{\xi^2}{k} \tag{17}$$

Equations (16) and (17) are the conservation equations of K and ε respectively where σ_{K1} and $\sigma_{\varepsilon1}$ are constants with values of 1.00 and 1.30. Based on the hydraulic diameter and Reynolds Number, the turbulence intensity (I_t), turbulence length scale (l), turbulent kinetic energy (K), dissipation rate (ε) was quantified using equation 18-21:

$$I_t = 0.16 \times (Re)^{-\frac{1}{8}} \tag{18}$$

$$l = 0.07 \times (Re) \tag{19}$$

$$K = \frac{3}{2}(V \times I)^2 \tag{20}$$

$$\varepsilon = C_\mu^{\frac{3}{4}} \times \frac{K^{\frac{3}{2}}}{l} \tag{21}$$

These data were employed in formulating the simulation model.

3.6 Methodology

A three-dimensional unsteady, hybrid solver with absolute velocity formulation was used for the study. The meshed model was imported to the Flow Simulation Module. SI units were used for the whole system and the type of analysis was marked as internal. The 'exclude cavity without flow separations' function was turned on. The RANS-based turbulence model employed in the FSM is a two-equation K-ε model based on earlier research (Driss *et al.* 2014; Putra, Noviani, & Muhardi. 2022). The model is known for its dependency on boundary layer separation and adverse pressure gradients around the blade wall. As suggested in section 3.2, the rotational region was defined as per (Saryazdi & Boroushaki. 2018; Ghiasi *et al.* 2021) and (Salari, Boushehri & Boroushaki. 2018). Water was selected as the fluid from the domain menu. The fluid properties, such as density and viscosity, were inherently called from the SolidWorks library. Based on the hydraulic diameter and Reynolds Number: the turbulence intensity, turbulent kinetic energy, and dissipation rate (as suggested by equations 18-21) were given as flow characteristics input. The default wall for the thermal condition was set as adiabatic with roughness as zero micrometres. The flow velocity was placed parallel to the Y direction (refer to Figure 8) and specified as 1.5m/s. Since the flow was set parallel to Y-axis, all components of gravity except the Z direction were set to zero. All velocity components (relative to rotating frame) except Y were set as zero.

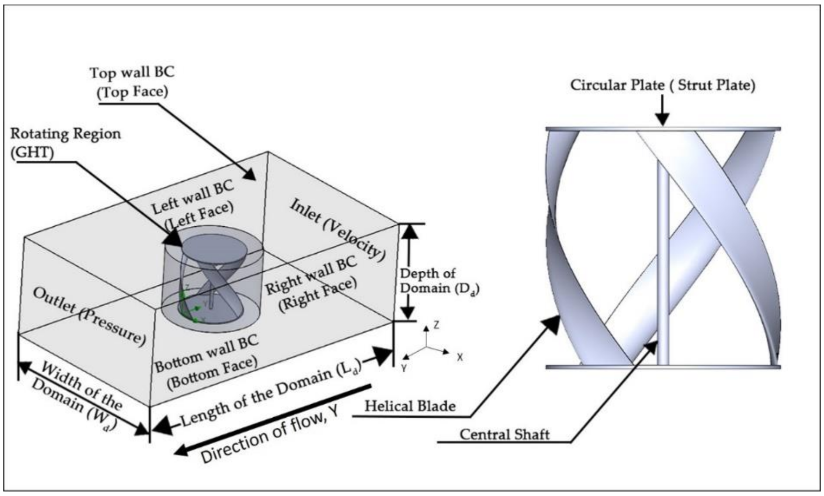

Fig. 8 Details of the computational domain and rotating region

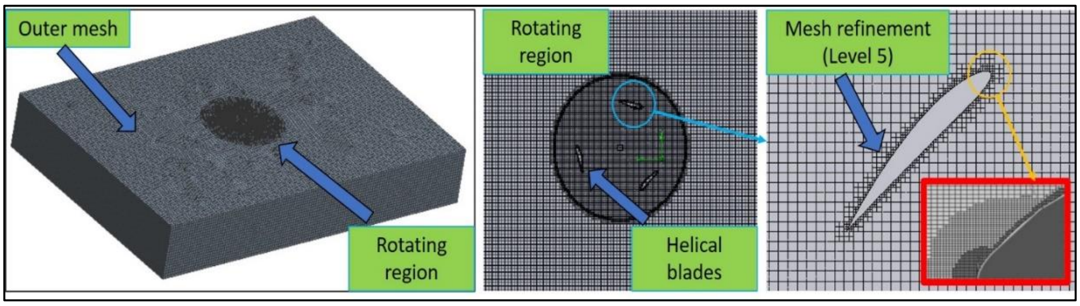

Fig 9 Details of mesh, rotational region and mesh refinement.

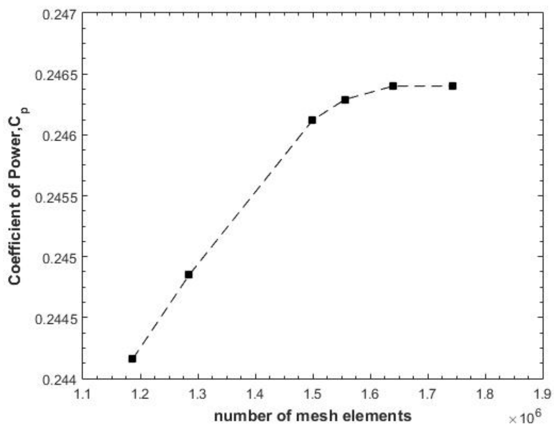

Fig 10. Mesh independency study (variation of C_p with respect to number of mesh elements)

Table 3
Configuration of mesh models

Mesh model	Number of mesh elements	C_p	Error percentage	Computation time (hh:mm:ss)*
K_1	1186922	0.24416	0.9006	05:12:17
K_2	1285109	0.24485	0.2129	05:57:07
K_3	1499780	0.24612	0.1041	06:41:37
K_4	1556050	0.24629	0.0327	07:07:41
K_5	1639761	0.246398	0.0332	07:57:34
K_6	1743910	0.246399	-	08:34:06

* i7 Intel (8th Gen)-32 GB RAM

The boundary conditions (as illustrated in Figure 8) of the inlet, outlet and side walls were inserted into corresponding fields. The fluid velocity (V_f =1.5 m/s) indicates the inlet boundary condition, and the zero-gauge pressure indicates the output boundary condition. No-slip boundary criteria was provided for the side walls. The parametric optimisation feature of SolidWorks was employed in FSM to simulate the nine turbines subjected to the same flow condition. The index of revolution of the turbine's switches to the next value as per the default algorithm whenever a meaningful convergence occurs. All necessary parameters, such as the force on blades, angular velocity, the torque of the turbine, etc., were selected under the 'goals' menu in the pre-processing operations.

The fluxes and pressure approximations that correspond to pressure-based and density-based techniques were blended on the faces of control volumes. These mixed estimates were substituted in a SIMPLE-type (Sobachkin & Dumnov. 2013) differencing technique. The original SIMPLE-type semi-implicit splitting scheme, the explicit density-based scheme, or a combination of these techniques can be obtained by controlling the mixing weight between the fluxes and pressure approximation. The convergence requirements for all residual formulas of continuity, momentum, and performance characteristics were defined as $1x10^{-6}$.

4. Experimentation

4.1 Fabrication of model

The model's skeleton (basic framework) was fabricated from a Cold Rolled (CR) iron sheet (Figure 11 A). The turbine's height was fixed as 0.600 m and diameter as 0.600 m, keeping the aspect ratio as unity. The chord length was 0.120 m. The index of revolution was decided to be 0.25 as per the simulations. The profile of the blade was NACA 4412. A dynamometer with a 12V rating was connected to the turbine using bearings (SKF0049). A similar bearing was employed at the other end of the shaft too. The skeleton of the model was fabricated, keeping the mean camber line of the aerofoil as a reference. Equally spaced lines were drawn perpendicular to the edges of the skeleton blade at regular intervals. A set of points on the line was identified, and ice-cream sticks with required heights were pasted at these locations to obtain the curvature resembling the aerofoil (Figure 11 B). Sealants were used to fill the space between the ice cream sticks (Figure 11 C). After leaving it out to dry for a day, the extra sealant was sanded. Twine thread was used to envelop the ice cream sticks. An adhesive binder was applied to the twine (Figure 11 D). A chromium-based primer (paint) coating, as illustrated in Figure 11 E, was applied to the turbine to improve its corrosion resistance. Finally, an additional layer of paint was applied to the turbine to improve its durability (Figure 11 F). A housing frame encloses the turbine for easy manoeuvrability.

4.2 Test rig

As illustrated in Figure 12, the experimental test ring consisted of GHT, Multimeters, Dynamo, and Housing. The rpm was measured using a digital laser-guided tachometer. Multimeters (Metravi P11) mounted on the top side of the turbine housing were used to measure the voltage and current of the dynamo. The test rig was placed in position using ropes which were subsequently removed. Plastic covers were used to protect the multimeters from getting wet throughout the experimentation.

Fig. 11 Various stages of manufacturing GHT

Reference	Description
1	Dynamo
2	Multimeter (Current)
3	Multimeter (Voltage)
4	Central shaft
5	Helical blade
6	Turbine housing (Frame)
7	Strut plate/disc

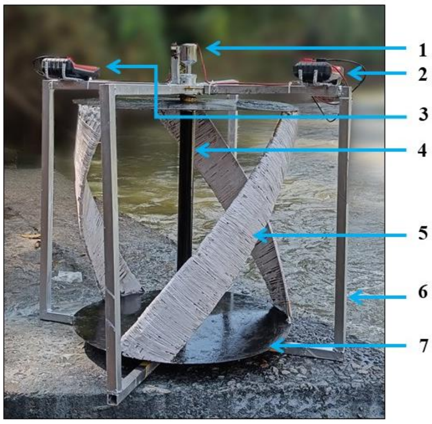

Fig 12 Schematic illustration of the test setup for GHT

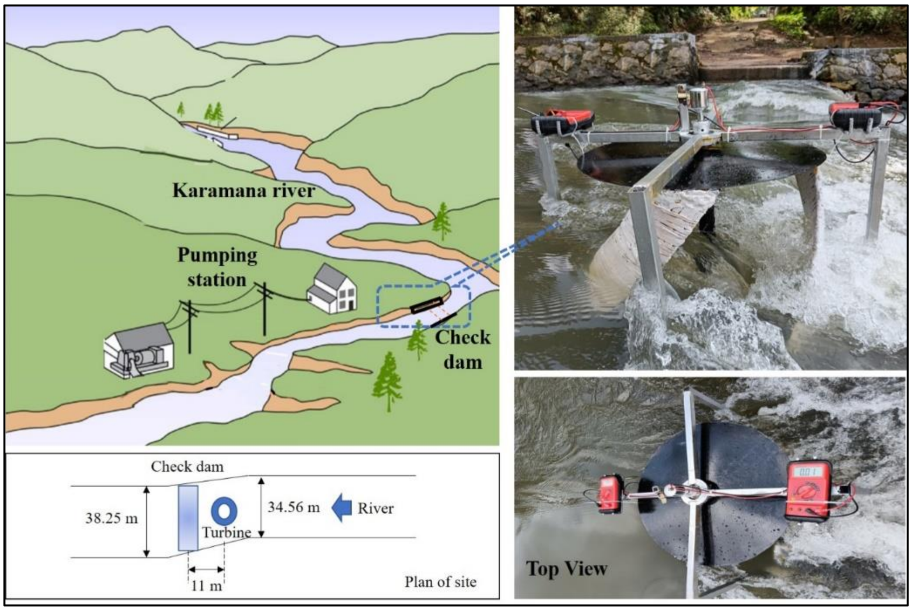

Fig. 13 Field testing and installation of GHT

Table 4
Data from experimentation

Index of revolution	Run Number	Current (A)	Voltage (V)	Power (W)	Rotation per minute
0.25	1	0.13	6	0.78	51
	2	0.12	5	0.60	50
	3	0.10	6.1	0.61	49
	4	0.11	5.9	0.64	51

4.3 Site selection and field testing

A suitable creek of the Karamana river was selected for field testing (Zhang *et al.* 2022) the GHT (refer to Figure 13). A check dam meant as a reservoir for the pump house is located here. The state-owned water pumping station has discharge and water velocity recorded (yearly basis). A current meter (Nixon 404, Propeller type) was used to measure the velocity of the stream. The check dam allows the reservoir to have a usable average depth of 0.65 m for effectively immersing the GHT. The upstream width of the check dam measures 34.56 m. The span of the check dam is 38.25 m. The turbine was located at 11 m from the check dam in the upstream direction (reservoir), where the velocity of the stream was 1.5 m/s. The turbine's output power was calculated from the recorded data. The following are the location coordinates of the experiment site: - 8° 34' 35.922" N (DMS Latitude) 77° 5' 18.1104" E (DMS Longitude). Table 4 gives the experimental data of GHT.

Table 5
Systematic error of measuring instruments

Experimental apparatus	Systematic error
Digital Multimeter (current measurement)	0.27 %
Digital Multimeter (voltage measurement)	0.10 %
Digital tachometer (laser based, non-contact)	3 %
Current meter	1 %

Table 6
Output characteristics of Gorlov Helical Turbine

Flow velocity of fluid at inlet (V_f) (m/s)	Index of revolution of GHT	Angular velocity of GHT (rad/s)	Force on GHT blades (N)	Torque generated by GHT (N m)	Output power (W)
1.5	0.10	0.822	0.614	0.638	0.524
	0.15	0.892	0.723	0.706	0.630
	0.20	0.887	0.921	0.823	0.730
	0.25	0.902	1.758	1.055	0.951
	0.30	0.898	0.932	0.714	0.641
	0.35	0.914	0.921	0.788	0.721
	0.40	0.882	0.736	0.622	0.548
	0.45	0.826	0.526	0.602	0.497
	0.50	0.842	0.514	0.542	0.456

5. Uncertainty analysis and systematic error

The uncertainty is calculated using Equations 22 and 23. These equations were obtained using (Moffat, 1988.) approach, and the uncertainty in output power measured was determined to be 2.68%.

$$P = VI \tag{22}$$

$$\frac{\partial P}{P} = \left[\left(\frac{\partial V}{V}\right)^2 + \left(\frac{\partial I}{I}\right)^2\right]^{\frac{1}{2}} \tag{23}$$

Table 5 summarises the systematic error associated with the various measuring devices considered in this research. Systematic error is a type of error that is constant and repetitive and is usually related to equipment or an experiment design. The systematic error values of the multimeters are well below the standard allowable limit prescribed by the manufacturer. The systematic error for the tachometer and current meter is in the acceptable range as defined by (Mosbahi *et al.* 2020) and (Talukdar, Kulkarni & Saha. 2018).

6. Results

6.1 Results from simulation

Nine GHTs with different indices of revolutions were subjected to a flow velocity of 1.5 m/s at the inlet. Table 6 presents the overall summary of the nine GHT's which were designed with different indices of revolution (0.10-0.50). The first two columns (from left) indicate the flow velocity and indices of revolution. These are the input parameters to the simulation model. The remaining columns (columns 3-6, from left) denote the output parameters from the simulation model. These include the angular velocity of the GHT, force on the helical blades, torque generated and output power of GHT. It is observed that for a flow velocity of 1.5 m/s, the GHT with the index of revolution of 0.25 develops a maximum output power of 0.951 W.

6.1.1 Variation of C_p (coefficient of power) with respect to TSR (Tip Speed Ratio)

The coefficient of power (C_p, refer equation 11) of a hydrokinetic turbine indicates the efficiency with which the turbine transforms the energy contained in the water to output power. Another critical measure for describing the turbine's performance is the Tip Speed Ratio (TSR, refer equation 12). TSR is the ratio of the turbine blade's tangential velocity to the fluid's flow velocity. Figure 14 (a-j) denotes the variation of C_p against TSR.

It is observed from Figure 14 (a-j) that the variation of TSR is from 0.525 to 1.275, and Cp is from 0.06 to 0.24. In Figure 14 (j), points for all turbines with indices of revolution from 0.10 to 0.50 are marked. These indicate that the turbine with an index of revolution of 0.25 has the best C_p of all. The C_p Vs TSR graphs illustrated typical patterns showcased in the studies of (Talukdar, Kulkarni & Saha. 2018) and (Bachant & Wosnik. 2015)

6.1.2 Velocity and pressure contours of GHT

Figure 15 depicts the variation of the linear velocity in the direction of flow of the fluid with respect to the turbine. The plot is of the GHT with 0.25 as the index of revolution. The flow lines near the turbine show a considerable reduction in velocity, which goes hand in hand with prediction. This means that the turbine blades utilise the dynamic pressure of the fluid. The top plane (XY plane) and side plane (YZ plane) is illustrated in Figure 15. The velocity plot is considered at the top and side midplanes. The fluid flow direction is as marked in Figure 15 (Y direction).

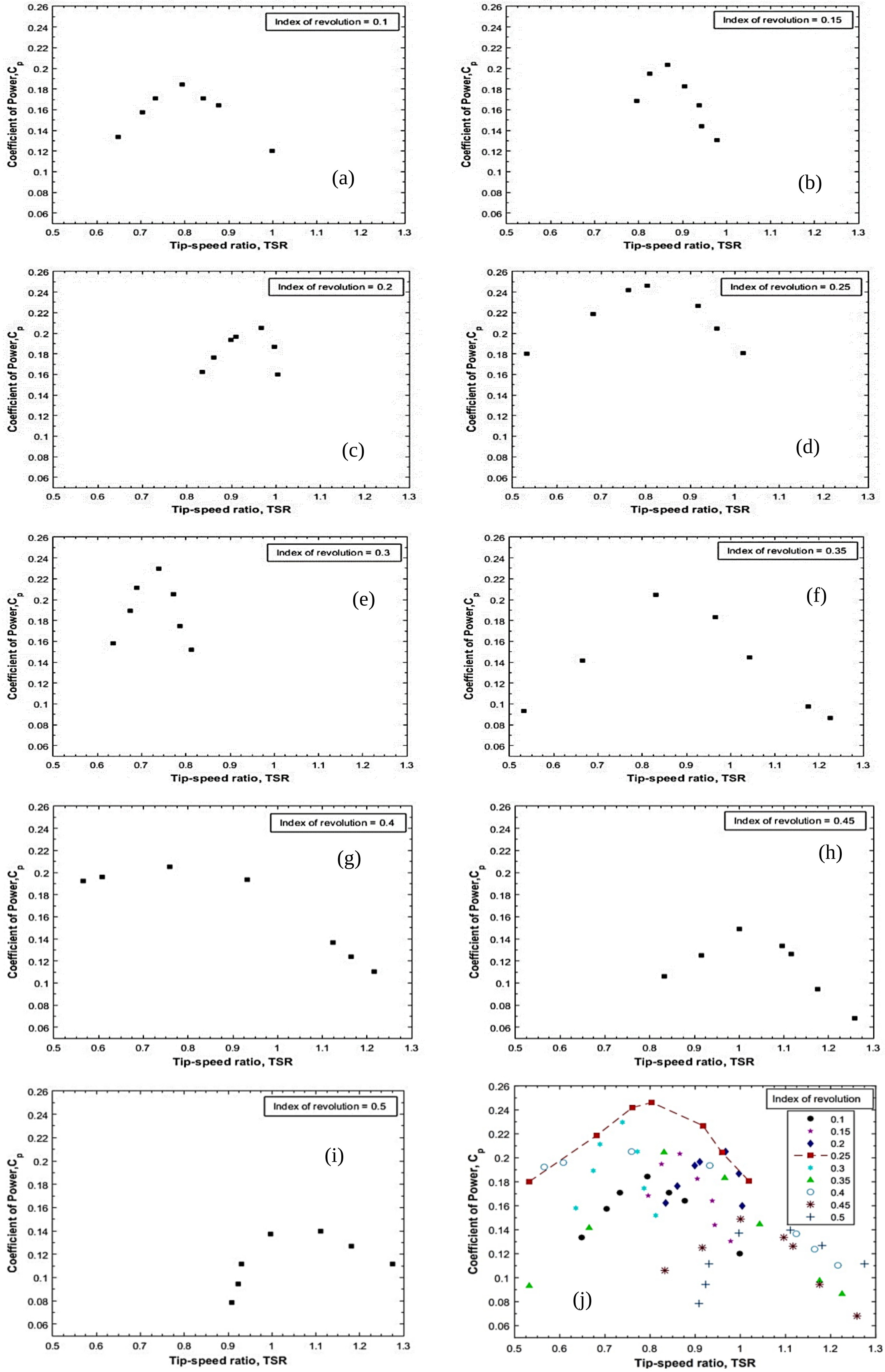

Fig. 14 (a-j) Variation of C_p with respect to TSR (Indices of revolution 0.1-0.5)

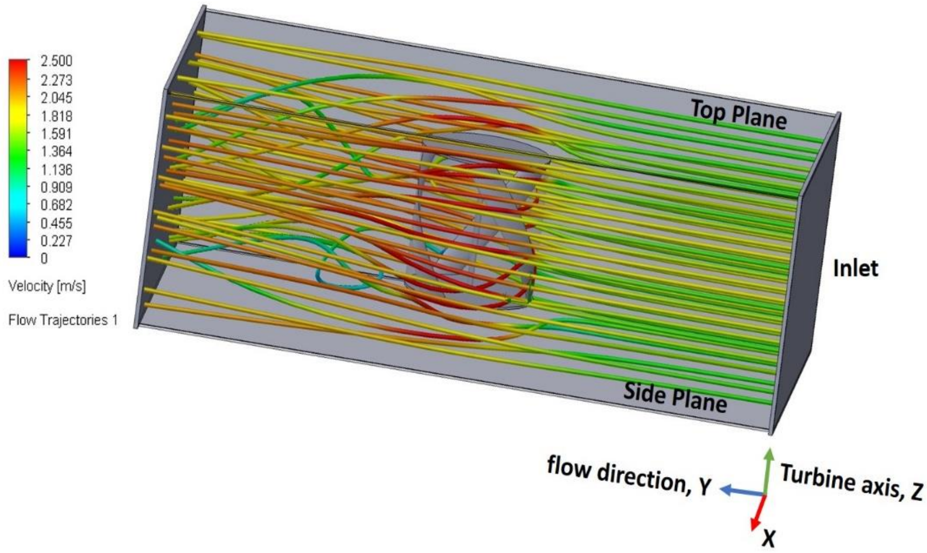

Fig 15 Linear velocity plots of turbine with 0.25 as index of revolution.

The velocity contours for GHT's (Figure 16 a-i) of different indices of revolution ranging from 0.1 to 0.5 is obtained against a flow of 1.5 m/s over the control volume. For the index of revolutions of 0.10 and 0.15, it can be observed on the side plane of velocity contour (Figure 16 a, b) that the GHT's acts more like a Darrieus turbine rather than exhibiting the flow characteristics of GHT. For this range of indices of revolution, flow velocity contrasts across the turbine may cause flow-induced vibrations. The scenario repeats for turbines with the index of revolution ranging from 0.35 to 0.50 (Figure 16 f-i). Hence the desirable range is shortened to the index of revolution of 0.20 to 0.30 (Figure 16 c-e). Here, the turbine with the index of revolution of 0.25 exhibits a stable velocity contour (Figure 16 d). The flow velocities are similar across the turbine. We observe maximum velocities on the top left and bottom right of the turbine blades.

On reviewing the top plane of velocity contour (Figure 16 d), it can be observed that the turbine model with the index of revolution of 0.25 exhibits a desirable velocity plot. Here, the blade's leading edges have maximum velocity. Further, the low-velocity contour is located farther from the incoming flow between the blades. Such a contour indicates smooth and effective rotation of the turbine since the leading edge is exposed to higher velocity and trailing blades are on lower flow velocity region. As the trailing blades have comparatively lower flow velocity, the angular velocity of the turbine would be optimum.

Figure 17 gives the variation of the dynamic pressure in the direction of the fluid flow with respect to the turbine. The plot is of the turbine with 0.25 as the index of revolution. The plot reveals the interaction of fluid particles with the turbine. The top plane (XY plane) and side plane (YZ plane) is illustrated in Figure 17. The pressure plot is considered at the top-midplane. The fluid flow direction is as marked in Figure 17 (Y direction).

The total pressure contour for GHT's (Figure 18 a-i) of different indices of revolution ranging from 0.1 to 0.5 is obtained against a flow of 1.5 m/s over the control volume.

In all cases, it can be observed that there is a drop in total pressure across the turbine. This pressure drop is converted into the rotation of the turbines. For turbines with indices of revolution of 0.1 and 0.15, it can be observed that low-pressure pockets occur on the leading surface of the blades (refer to Figure 18 a, b). Here the rotation of the blades is attributed to the pressure difference between the outer and inner surfaces of the blades. For turbines with an index of revolution of 0.20, high pressure builds up in the leading edge (refer to Figure 18c). Lower pressure occurs on the trailing surface of the blades. The drag force so developed generates the necessary torque on the turbine.

The high-pressure drop on the leading-edge is maximum for the turbine with an index of revolution of 0.25. These desired pressure contours (refer to Figure 18 d) suggest that the turbine with an index of revolution of 0.25 is the best in class. However, for turbines with indices of revolution of 0.30 and above (refer to Figure e-i), a high-pressure pocket can be observed on the leading, trailing edges and lower surface of the blade (below the chord line) (Figure e). Lower pressure occurs on the blade's upper surface (above the chord line) (Figure e). Such a pressure pattern tends to disrupt the mechanical stability of the blades. Thus, the pressure difference would induce bending stresses on the blade rather than rotation.

Table 7
Comparison of output power

Index of revolution	Output power (Analytical)	Output power (Simulation)	Output power (Experimentation)
0.25	1.11 W	0.951 W	0.65 W (Average Value)

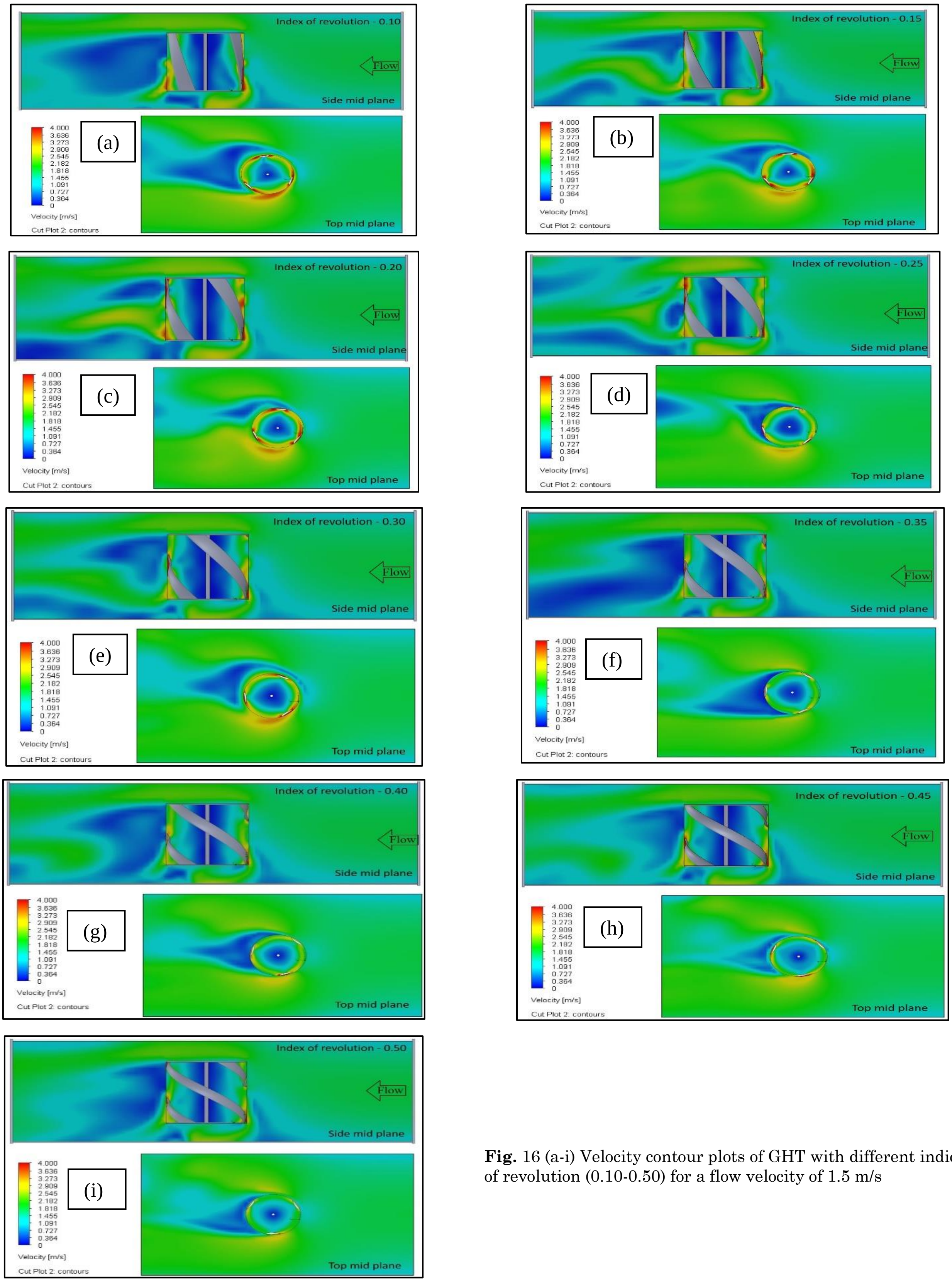

Fig. 16 (a-i) Velocity contour plots of GHT with different indices of revolution (0.10-0.50) for a flow velocity of 1.5 m/s

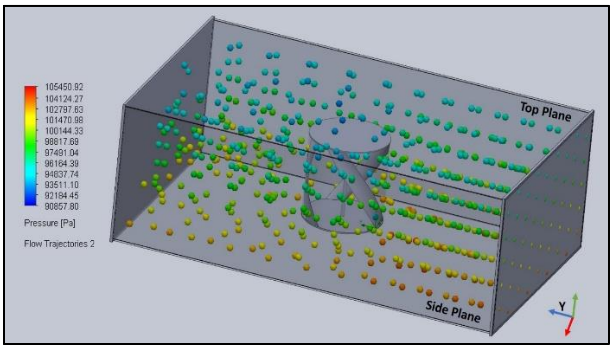

Fig. 17 Trajectory and dynamic pressure plot of the turbine with 0.25 as the index of revolution.

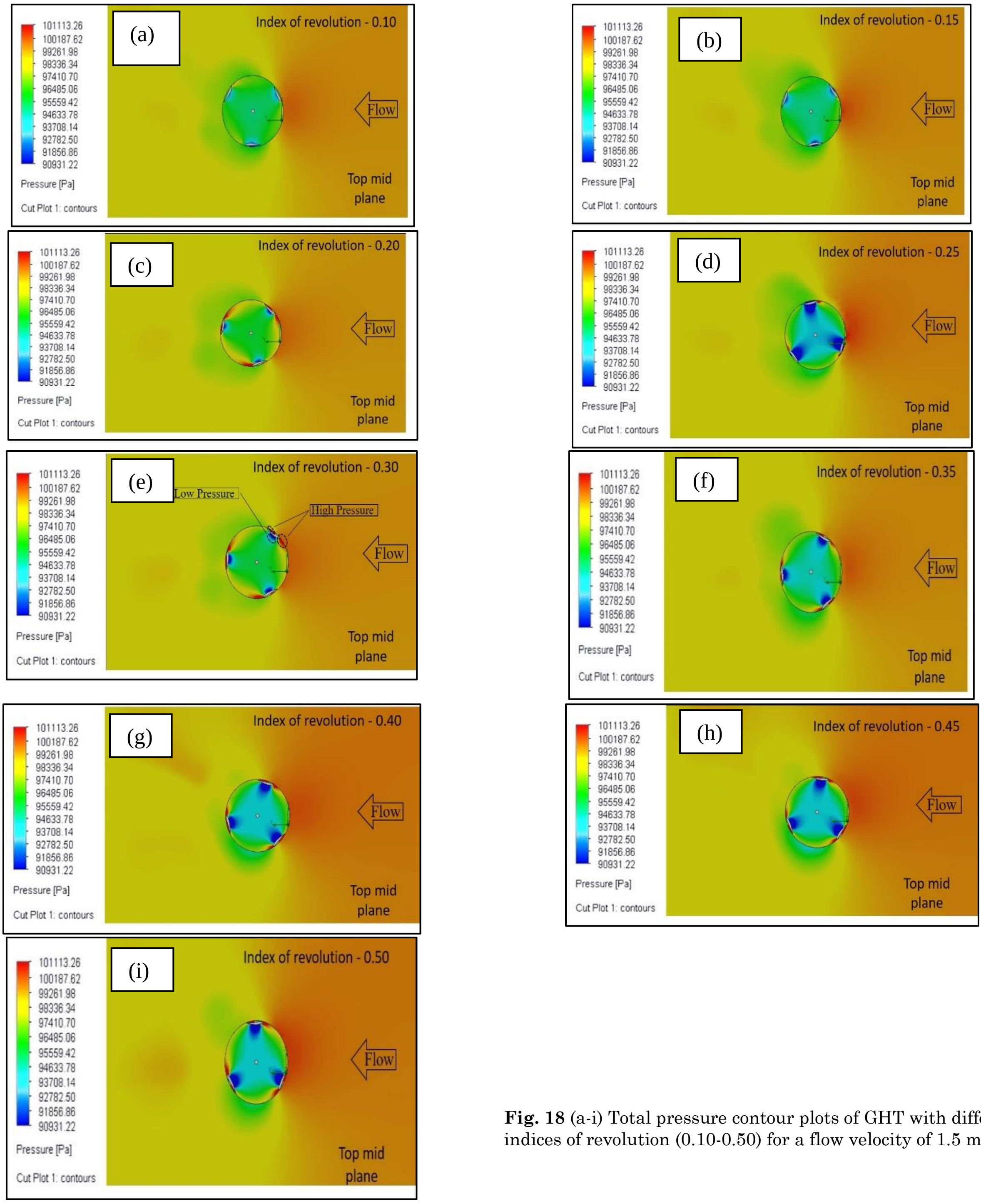

Fig. 18 (a-i) Total pressure contour plots of GHT with different indices of revolution (0.10-0.50) for a flow velocity of 1.5 m/s

6.2 Results from experimentation

Nine GHT models with different indices of revolution varying from 0.10 to 0.50 for power generation were studied using computation tools. The one with 0.25 as the index of revolution was found good enough for prototype development. Table 4 in section 4.3 provides the experimental data of the GHT. The turbine could self-start and generate power when introduced into the river creek. Table 7 compares the power developed by the turbine in closed-form (analytical), simulation and experimentation. In experimentation, the prototype developed 0.65 W, 30% less than the value obtained through simulation. The mechanical loss as suggested by (Yun *et al.* 2010), profile geometry, and heaviness attribute to the mismatch. Optimising multiple parameters using parametric modelling and an allied algorithm such as a genetic algorithm could yield better insight into this problem (Pourrajabian, Dehghan & Rahgozar. 2021). The studies suggest a viable solution for the struggling Small Hydro Power (SHP) sector, primarily from untapped potentials such as tailrace and runoff water. Integrating smart grids into these sectors is essential.

7. Conclusion

The study aimed at investigating the parametric optimisation of the Gorlov Helical Turbine with respect to the index of revolution. The effect of the index of revolution on the output power of the turbine was studied using simulation and further verified using experimentation supported by closed-form solutions. Nine GHT models were created using SolidWorks modelling software with different indices of revolution (from 0.10 to 0.50, with a step size of 0.05). SolidWorks Flow Simulation Module (FSM) models a three-dimensional simulation equivalent to an open channel of a river creek.

Studies suggest varying the indices of revolution of the helical blades affects the turbine's output power. Turbine with 0.25 as the index of revolution offered better output power than others. The coefficient of power values for GHT with 0.25 as the index of revolution was higher relative to other turbines for flow velocity varying from 1.1 m/s to 1.7m/s. The turbine with 0.25 as the index of revolution exhibits a desirable velocity contour. The flow velocities are similar across the turbine. Maximum velocities are observed on turbine blades' top left and bottom right. The desired total pressure contour suggests that the turbine with an index of revolution of 0.25 is the best in class. For turbines with indices of revolution of 0.30 and above, a high-pressure pocket can be observed on the leading, trailing edges and lower surface of the blade (below the chord line). Lower pressure occurs on the blade's upper surface (above the chord line). Such a pressure pattern tends to disrupt the mechanical stability of the blades. The output power of the turbine was also analytically calculated using Gavasheli's formula for TSR=1. The actual output power as per the formula is 1.11 W, which is comparable to the output power by simulation (0.951 W).

Further, a model of the best configuration as determined through simulation runs was fabricated and tested. The prototype developed 0.65 W against a flow velocity of 1.5 m/s, 30% less than the value obtained through simulation. The mismatch can be attributed to the mechanical loss. The unsymmetrical profile of the blade makes it challenging to fabricate using traditional techniques. Thus, 3D printing would be an apt technology for manufacturing such blades.

Acknowledgements

The authors would like to thank the Kerala Water Authority (India) for providing necessary aid in experimentation. This research did not receive any specific grant from funding agencies in the public, commercial, or not-for-profit sectors.

Abbreviations

GHT	- Gorlov Helical Turbine.
SHP	- Small Hydro Power plant.
H-Darrieus	- Horizontal axis Darrieus water turbine.
NACA	- National Advisory Committee for Aeronautics.
TSR	- Tip Speed Ratio.
AR	- Aspect Ratio.
FSM	- Flow Simulation Module.
QUAD	- Four Nodes quadrilaterals or hexahedral elements.
FVM	- Finite volume method.
NS	- Navier-Stokes equation.
RANS	- Reynold Averaged Navier-Stokes
CR	- Cold Rolled.
DMS	- Degrees Minutes and Seconds.
3D	- Three-dimensional

Nomenclature

σ	– Relative solidity.
n, N	– Denotes the number of blades.
b	– Chord of each blade cross-section, m.
D	– Diameter of the turbine, m.
H	– Height of the turbine, m.
r	– Radius of the turbine, m.
d	– Half of the blade's chord in radians with respect to the axis of rotation, rad.
C_L	– Coefficient of Lift as per NACA.
C_d	– Coefficient of drag as per NACA.
C_p	– Coefficient of power
α	– Angle of attack.
ρ	– Density of water, kg/m^3.
A	– Projected area of the turbine, m^2.
V_f	– velocity of the fluid, m/s.
V	– Voltage, V.
F	–Tangential force on the turbine, N.
T	– Torque developed by the turbine, N m.
λ	– Tip speed ratio (TSR).
ω	– Angular velocity of the turbine, rad/s.
P	– Power developed by the turbine, W.
I_t	– Turbulence Intensity.
I	– Current, A.
l	–Turbulence length scale, m.
Re	– Reynolds number.
K	– Turbulent kinetic energy, m^2/s^2.
ε	– Turbulence dissipation rate, m^2/s^3.
C_μ	– Empirical constant, having an approximate value of 0.09.
η_m	–Efficiency of gearbox.
η_e	– Efficiency of generator.

References

Akhatova, A., Kassymov, A., Kazmaganbetova, M., & Rojas-Solórzano, L. (2015). CFD simulation of the dispersion of exhaust gases in a traffic-loaded street of Astana, Kazakhstan. *Journal of Urban and Environmental Engineering*, 9(2), 158–166. https://doi.org/10.4090/juee.2015.v9n2.158166

Al-Dabbagh, M. A., & Yuce, M. I. (2019). Numerical evaluation of helical hydrokinetic turbines with different solidities under different flow conditions. *International Journal of Environmental Science and Technology*, 16(8), 4001–4012. https://doi.org/10.1007/s13762-018-1987-1

Al-Dabbagh, Mohammad A., & Yuce, M. I. (2018). Simulation and comparison of helical and straight-bladed hydrokinetic turbines. *International Journal of Renewable Energy Research,* 8(1), 504–513. https://www.ijrer.org/ijrer/index.php/ijrer/article/view/6697

Anderson, J., Stelzenmuller, N., Hughes, B., Johnson, C., Taylor, B., Sutanto, L., Mcquaide, E., & Polagye, B. (2011). Design and Manufacture of a Cross-Flow Helical Tidal Turbine. http://depts.washington.edu/pmec/docs/20110615_ME495_report_Micropower.pdf

Bachant, P., & Wosnik, M. (2011). Experimental investigation of helical cross-flow axis hydrokinetic turbines, including effects of waves and turbulence. *Proceedings of the ASME-JSME-KSME 2011 Joint Fluids Engineering Conference*, 1–12. https://tethys.pnnl.gov/sites/default/files/publications/Bachant-and-Wosnik-2011.pdf

Bachant, P., & Wosnik, M. (2015). Performance measurements of cylindrical- and spherical-helical cross-flow marine hydrokinetic turbines, with estimates of exergy efficiency. *Renewable Energy*, 74, 318–325. https://doi.org/10.1016/j.renene.2014.07.049

Berhanu, H., Gudeta, D., Haiter Lenin, A., & Karthikeyan, B. (2020). Numerical and experimental investigation of an exhaust air energy recovery Savonius wind turbine for power production. *Materials Today: Proceedings*, 46(9), 4142–4152. https://doi.org/10.1016/j.matpr.2021.02.675

Camocardi, M., Marañon, J., Delnero, J., & Colman, J. (2011). Experimental Study of a Naca 4412 Airfoil With Movable Gurney Flap. 47(January), 1–15. https://doi.org/10.2514/6.2011-1309

Chakka, M. (2016). Gorlov Helical Turbine and the process of Energy Generation Under graduate project report. Shiv Nadar University, India. https://doi.org/10.13140/RG.2.1.2555.8642

De Oliveira, B. L., & Sundnes, J. (2016). Comparison of tetrahedral and hexahedral meshes for finite element simulation of cardiac electro-mechanics. ECCOMAS Congress 2016 - *Proceedings of the 7th European Congress on Computational Methods in Applied Sciences and Engineering*, 1(June), 164–177. https://doi.org/10.7712/100016.1801.9193

Driss, Z., Mlayeh, O., Driss, D., Maaloul, M., & Abid, M. S. (2014). Numerical simulation and experimental validation of the turbulent flow around a small incurved Savonius wind rotor. *Energy,* 74(C), 506–517. https://doi.org/10.1016/j.energy.2014.07.016

Ghiasi, P., Najafi, G., Ghobadian, B., & Jafari, A. (2021). Analytical and numerical solution for H-type darrieus wind turbine performance at the tip speed ratio of below one. *International Journal of Renewable Energy Development*, 10(2), 269–281. https://doi.org/10.14710/ijred.2021.33169

Gorlov, Alexander M. (1998). Helical Turbines for the Gulf Stream: Conceptual Approach to Design of a Large-Scale Floating Power Farm. *Mar Technol SNAME N* 35 175–182. https://doi.org/10.5957/mt1.1998.35.3.175

Gorlov, A.M. (1995). The helical turbine: A new idea for low-head hydro. *Hydro Review*, 14.

Jayaram, V., & Bavanish, B. (2018). Viability study of implementing cross flow helical turbine for micropower generation in India. *International Journal of Renewable Energy Research*, 8(1), 274–279. https://doi.org/10.20508/ijrer.v8i1.6744.g7301

Jayaram, V., & Bavanish, B. (2020). A brief review on the Gorlov helical turbine and its possible impact on power generation in India. Materials Today: *Proceedings*, 37(Part 2), 3343–3351. https://doi.org/10.1016/j.matpr.2020.09.203

Kirke, B. K. (2011). Tests on ducted and bare helical and straight blade Darrieus hydrokinetic turbines. *Renewable Energy*, 36(11), 3013–3022. https://doi.org/10.1016/j.renene.2011.03.036

Kumar, R., Singal, S. K., Dwivedi, G., & Shukla, A. K. (2020). Development of maintenance cost correlation for high head run of river small hydro power plant. *International Journal of Ambient Energy,* 0(0), 1–38. https://doi.org/10.1080/01430750.2020.1804447

Letchumanan, S. M., Tajul Arifin, A. M., Taib, I., Rahim, M. Z., & Nor Salim, N. A. (2021). Simulating the Optimization of Carbon Fiber Reinforced Polymer as a Wrapping Structure on Piping System Using SolidWorks. *Journal of Failure Analysis and Prevention*, 21(6), 2038–2063. https://doi.org/10.1007/s11668-021-01287-4

Moffat, R. J. (1988). Describing the uncertainties in experimental results. *Experimental Thermal and Fluid Science*, 1(1), 3–17. https://doi.org/10.1016/0894-1777(88)90043-X

Mosbahi, M., Ayadi, A., Chouaibi, Y., Driss, Z., & Tucciarelli, T. (2020). Experimental and numerical investigation of the leading edge sweep angle effect on the performance of a delta blades hydrokinetic turbine. *Renewable Energy*, 162, 1087–1103. https://doi.org/10.1016/j.renene.2020.08.105

Mrigua, K., Toumi, A., Zemamou, M., Ouhmmou, B., Lahlou, Y., & Aggour, M. (2020). Cfd investigation of a new elliptical-bladed multistage savonius rotors. *International Journal of Renewable Energy Development*, 9(3), 383–392. https://doi.org/10.14710/ijred.2020.30286

Mwaniki, G. R., Okok, M. O., & Oromat, E. (2019). Expanding access to clean energy in developing countries: The role of off-grid mini hydro power projects in Kenya. *International Journal of Renewable Energy Research*, 9(3), 1571–1577. https://doi.org/10.20508/ijrer.v9i3.9486.g7746

Pongduang, S., Kayankannavee, C., & Tiaple, Y. (2015). Experimental Investigation of Helical Tidal Turbine Characteristics with Different Twists. In *Energy Procedia* (Vol. 79). Elsevier B.V. https://doi.org/10.1016/j.egypro.2015.11.511

Pourrajabian, A., Dehghan, M., & Rahgozar, S. (2021). Genetic algorithms for the design and optimization of horizontal axis wind turbine (HAWT) blades: A continuous approach or a binary one? *Sustainable Energy Technologies and Assessments*, 44(September 2020), 101022. https://doi.org/10.1016/j.seta.2021.101022

Prabhu, L., Krishnamoorthi, S., Gokul, P., Sushan, N., Hisham Harshed, P. H., & Jose, A. (2020). Aerodynamics analysis of the car using solidworks flow simulation with rear spoiler using CFD. *IOP Conference Series: Materials Science and Engineering*, 993(1). https://doi.org/10.1088/1757-899X/993/1/012002

Price, M. A., & Armstrong, C. G. (1997). Hexahedral mesh generation by medial surface subdivision: Part ii. solids with flat and concave edges. *International Journal for Numerical Methods in Engineering*, 40(1), 111–136. https://doi.org/10.1002/nme.1620381910

Putra, Y. S., Noviani, E., & Muhardi, M. (2022). Numerical Study of The Effect of Penstock Dimensions on a Micro-hydro System using a Computational Fluid Dynamics Approach. *International Journal of Renewable Energy Development*, 11(2), 491–499. https://doi.org/10.14710/ijred.2022.42343

Ragoth Singh, R., & Nataraj, M. (2014). Design and analysis of pump impeller using SWFS. *World Journal of Modelling and Simulation,* 10(2), 152–160. http://www.worldacademicunion.com/journal/17467233WJMS/wjmsvol10no02paper08.pdf

Rezaeiha, A., Kalkman, I., & Blocken, B. (2017). CFD simulation of a vertical axis wind turbine operating at a moderate tip speed ratio: Guidelines for minimum domain size and azimuthal increment. *Renewable Energy*, 107, 373–385. https://doi.org/10.1016/j.renene.2017.02.006

Salari, M. S., Boushehri, B. Z., & Boroushaki, M. (2018). Aerodynamic analysis of backward swept in hawt rotor blades using CFD. *International Journal of Renewable Energy Development*, 7(3), 241–249. https://doi.org/10.14710/ijred.7.3.241-249

Saryazdi, S. M. E., & Boroushaki, M. (2018). 2D numerical simulation and sensitive analysis of H-darrieus wind turbine. *International Journal of Renewable Energy*

Development, 7(1), 23–34. https://doi.org/10.14710/ijred.7.1.23-24
Shashikumar, C.M., Honnasiddaiah, R., Hindasageri, V., & Madav, V. (2021a). Experimental and numerical investigation of novel V-shaped rotor for hydropower utilization. *Ocean Engineering*, 224, 108689. https://doi.org/10.1016/j.oceaneng.2021.108689
Shashikumar, C.M., Honnasiddaiah, R., Hindasageri, V., & Madav, V. (2021b). Studies on application of vertical axis hydro turbine for sustainable power generation in irrigation channels with different bed slopes. *Renewable energy*, 163(2021), 845-857. https://doi.org/10.1016/j.renene.2020.09.015.
Shashikumar, C.M., & Madav, V. (2021). Numerical and experimental investigation of modified V-shaped turbine blades for hydrokinetic energy generation. *Renewable Energy*, 177, 1170–1197. https://doi.org/10.1016/j.renene.2021.05.086
Shiono, M., Suzuki, K., & Kiho, S. (2002). Output Characteristics of Darrieus Water Turbine with Helical Blades for Tidal Current Generations. Proceedings of the International Offshore and Polar Engineering Conference, 12, 859–864.
Sobachkin, A., & Dumnov, G. (2013). Numerical Basis of CAD-Embedded CFD. NAFEMS World Congress 2013, February, 1–20. https://www.solidworks.com/sw/docs/flow_basis_of_cad_embedded_cfd_whitepaper.pdf
Supreeth, R., Arokkiaswamy, A., Raikar, N. J., & Prajwal, H. P. (2019). Experimental investigation of performance of a small-scale horizontal axis wind turbine rotor blade. *International Journal of Renewable Energy Research*, 9(4), 1983–1994. https://www.ijrer.org/ijrer/index.php/ijrer/article/download/9898/pdf
Talukdar, P. K., Kulkarni, V., & Saha, U. K. (2018). Field-testing of model helical-bladed hydrokinetic turbines for small-scale power generation. *Renewable Energy*, 127, 158–167. https://doi.org/10.1016/j.renene.2018.04.052
Yagmur, S., Kose, F., & Dogan, S. (2021). A study on performance and flow characteristics of single and double H-type Darrieus turbine for a hydro farm application. *Energy Conversion and Management*, 245, 114599. https://doi.org/10.1016/j.enconman.2021.114599
Yun, Z., Kun, G. Y., Xiang, Z. L., Mao, X. T., & Kui, D. H. (2010). Torque model of hydro turbine with inner energy loss characteristics. *Science China Technological Sciences*, 53(10), 2826–2832. https://doi.org/10.1007/s11431-010-4098-x
Zanette, J., Imbault, D., & Tourabi, A. (2010). A design methodology for cross flow water turbines. *Renewable Energy,* 35(5), 997–1009. https://doi.org/10.1016/j.renene.2009.09.014
Zhang, A., Liu, S., Ma, Y., Hu, C., & Li, Z. (2022). Field tests on model efficiency of twin vertical axis helical hydrokinetic turbines. *Energy,* 247. https://doi.org/10.1016/j.energy.2022.123376